

Backbone amides are determinants of Cl⁻ selectivity in CLC ion channels

Received: 30 June 2022

Accepted: 23 November 2022

Published online: 06 December 2022

Check for updates

Lilia Leisle¹, Kin Lam^{2,3,4,5,6}, Sepehr Dehghani-Ghahnaviyeh^{2,3,4,5,6},
Eva Fortea^{1,7}, Jason D. Galpin⁸, Christopher A. Ahern⁸,
Emad Tajkhorshid^{2,3,4,5,6} & Alessio Accardi^{1,7,9} ✉

Chloride homeostasis is regulated in all cellular compartments. CLC-type channels selectively transport Cl⁻ across biological membranes. It is proposed that side-chains of pore-lining residues determine Cl⁻ selectivity in CLC-type channels, but their spatial orientation and contributions to selectivity are not conserved. This suggests a possible role for mainchain amides in selectivity. We use nonsense suppression to insert α -hydroxy acids at pore-lining positions in two CLC-type channels, CLC-0 and bCLC-k, thus exchanging peptide-bond amides with ester-bond oxygens which are incapable of hydrogen-bonding. Backbone substitutions functionally degrade inter-anion discrimination in a site-specific manner. The presence of a pore-occupying glutamate side chain modulates these effects. Molecular dynamics simulations show backbone amides determine ion energetics within the bCLC-k pore and how insertion of an α -hydroxy acid alters selectivity. We propose that backbone-ion interactions are determinants of Cl⁻ specificity in CLC channels in a mechanism reminiscent of that described for K⁺ channels.

Anion-selective channels and transporters control Cl⁻ homeostasis in all living cells and within their intracellular compartments. The ability of these channels to select against cations and discriminate amongst physiological anions is central to their function in vivo. While cation selectivity mechanisms are relatively well understood^{1–8}, the principles underlying Cl⁻ channel selectivity are poorly resolved. Indeed, most ‘Cl⁻ channels’ are more permeable to anions other than their biological namesake: GABA⁹, CFTR¹⁰, TMEM16A¹¹, TMEM16B¹², and Bestrophin^{13,14} channels follow the Hofmeister lyotropic selectivity sequence¹⁵ of SCN⁻>I⁻>NO₃⁻>Br⁻>Cl⁻, with slight deviations. In contrast, CLC-type channels and transporters select for Cl⁻ over other anions with a sequence of Cl⁻>Br⁻>NO₃⁻>I⁻^{16–21}. This selectivity sequence is evolutionarily well-conserved from prokaryotes to

eukaryotes and between transporters and channels. While most CLCs are Cl⁻ selective, the atCLC-a exchanger from *Arabidopsis thaliana* is NO₃⁻ selective^{22,23}, and members of a clade of prokaryotic CLCs are highly F⁻ selective^{24–27}. Thus, the CLC pore provides a unique and plastic structural template to investigate the mechanisms that underlie anion selectivity.

All CLCs are dimers, where each monomer forms a separate Cl⁻ permeation pathway^{28,29}. The CLC-ec1 structure allowed for the identification of three anionic binding sites^{30–37}, coined S_{int}, S_{cen} and S_{ext} for internal, central and external, respectively (Fig. 1A–C), whose position and coordination are evolutionarily conserved in eukaryotic channels and transporters. Coordination with permeant anions at the internal S_{int} site is weak as the dehydration of ions is

¹Department of Anesthesiology, Weill Cornell Medical College, New York, NY, USA. ²Theoretical and Computational Biophysics Group, University of Illinois at Urbana-Champaign, Urbana, IL 61801, USA. ³NIH Center for Macromolecular Modeling and Bioinformatics, University of Illinois at Urbana-Champaign, Urbana, IL 61801, USA. ⁴Beckman Institute for Advanced Science and Technology, University of Illinois at Urbana-Champaign, Urbana, IL 61801, USA. ⁵Department of Biochemistry, University of Illinois at Urbana-Champaign, Urbana, IL 61801, USA. ⁶Center for Biophysics and Quantitative Biology, University of Illinois at Urbana-Champaign, Urbana, IL 61801, USA. ⁷Department of Physiology and Biophysics, Weill Cornell Medical College, New York, NY, USA. ⁸Department of Molecular Physiology and Biophysics, University of Iowa, Iowa City, IA, USA. ⁹Department of Biochemistry, Weill Cornell Medical College, New York, NY, USA.

✉ e-mail: ala2022@med.cornell.edu

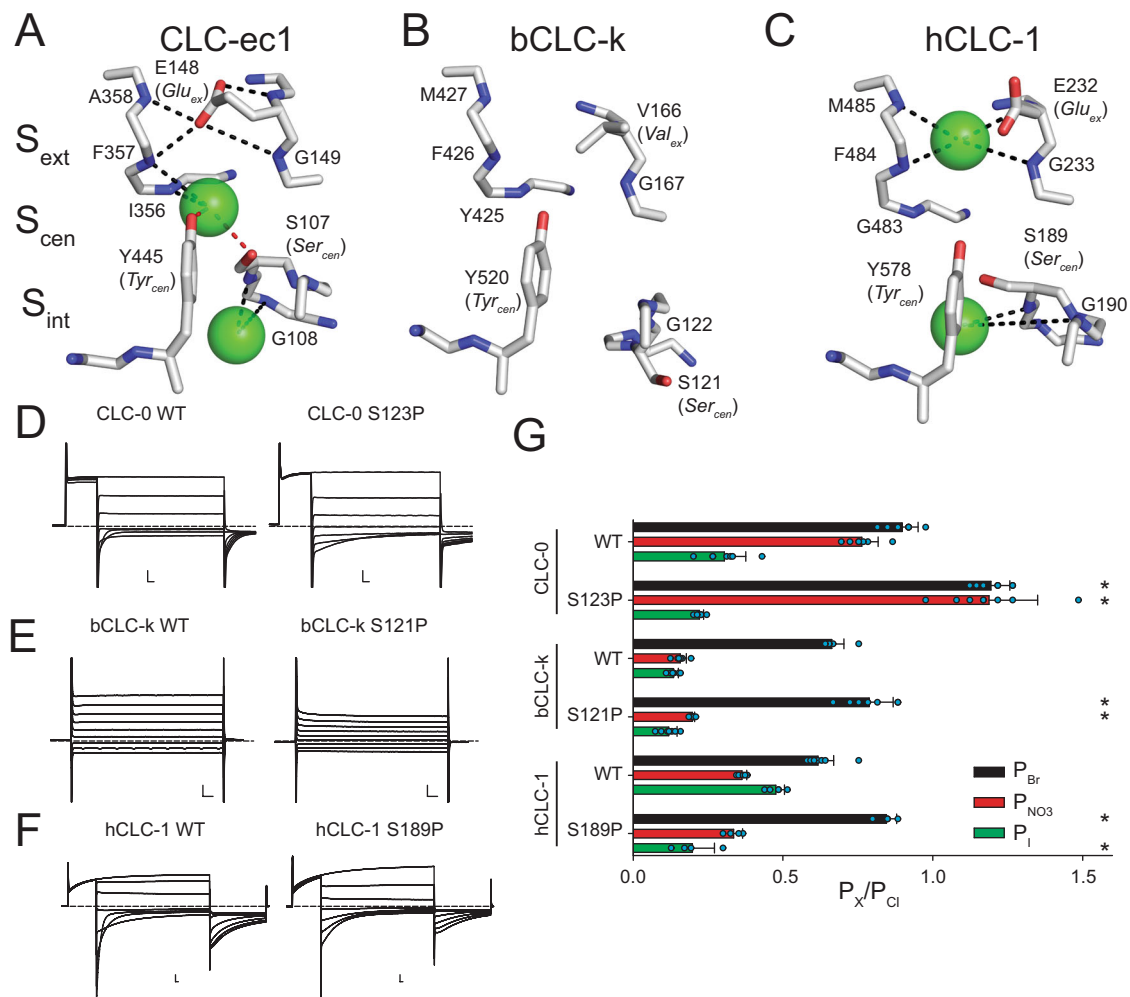


Fig. 1 | Structural architecture and ion coordination in the Cl^- pathway of CLC channels and transporters. Close up view of the Cl^- permeation pathway in CLC-ec1 (PDB: 1OTS, **A**), bCLC-k (PDB: 5TQQ, **B**) and CLC-1 (PDB: 6COY, **C**). The position of the external (S_{ext}), central (S_{cen}) and internal (S_{int}) binding sites is identified based on the crystal structure of CLC-ec1³¹. Bound Cl^- ions are shown as green spheres. No ions were resolved in the bCLC-k structure³³. Dashed lines indicate hydrogen bonds between the Cl^- ions and side chains (red) or backbone amides (black)^{31,34}. Representative current traces of WT and proline mutants at Ser_{cen} in CLC-0 (**D**), bCLC-k (**E**) and hCLC-1 (**F**). Dashed lines indicate the 0 current level.

Scale bars indicate 2 μA and 10 ms. **G** The relative permeability ratios for Br^- , NO_3^- and I^- of CLC-0 (WT and S123P), bCLC-k (WT and S121P) and hCLC-1 (WT and S189P). Data are Mean \pm St.Dev. of $n > 4$ repeats from $N \geq 3$ independent oocyte batches, individual data points are shown as cyan circles. The statistical significance of the effects of the mutants on the permeability ratios of each ion (indicated by *) was evaluated with a one-sided Student's t-test with a Bonferroni correction (see Methods). Mean values and p-values are reported in Supplementary Table 1. Individual data points are shown grouped by ion in Supplementary Fig. 5. Raw data for **D–G** and Fig. 2B, C is included in the Source Data Files.

only partially compensated via interactions with the backbone amides of a serine residue at position 107 (called Ser_{cen}) and Glycine 108 (using CLC-ec1 numbering) in the loop connecting helices C and D (Fig. 1A, C)^{19,30,38}. Conversely, anions positioned in the central and external sites, S_{cen} and S_{ext} , interact with the protein more extensively, consistent with a key role of this region in selectivity. In S_{cen} , Cl^- is coordinated by the conserved side chains of S107 (Ser_{cen}) and of Y445 (Tyr_{cen}), as well as the backbone amides of I356 and F357 (Fig. 1A). Ion coordination in S_{ext} is mediated by the backbone amides of E148 (Glu_{ex}), G149, F357 and A359 (Fig. 1A). Thus, interactions with side chains and backbone amides contribute to the preferential stabilization of anions over cations within the CLC pore^{31,39}. This pore architecture is conserved in the mammalian bCLC-k and hCLC-1 channels, involving similar coordination patterns (Fig. 1B, C), with the notable exception that in bCLC-k Ser_{cen} points away from S_{cen} (Fig. 1B) and that mutations at Ser_{cen} in the human CLC-Ka channel do not affect selectivity⁵³, recently led to the proposal that other pore-lining side chains are important for anion specificity. However, while side chains are not conserved, the functional preservation of the anion selectivity sequence points to a shared mechanism between hCLC-Ka and other CLC channels and transporters.

Supplementary Fig. 1). The competition between Glu_{ex} and the Cl^- ions is essential for CLC function^{28,29,32,40–42} and weakened ion binding at the S_{cen} site alters Cl^-/H^+ exchange stoichiometry in the transporters and gating in channels^{17,20,43–49}. Thus, the molecular and energetic determinants of selective anion binding and permeation also govern the CLC transport mechanism.

The current consensus mechanism for CLC selectivity is that the S_{cen} site is the primary regulator of anion discrimination and that the side chain of Ser_{cen} is the critical determinant of its specificity, as proline mutations at this site switch the selectivity from Cl^- to NO_3^- and vice versa^{17,19–21,23,50–52}. However, the recent finding that in bCLC-k channel Ser_{cen} points away from S_{cen} ³³ (Fig. 1B) and that mutations at Ser_{cen} in the human CLC-Ka channel do not affect selectivity⁵³, recently led to the proposal that other pore-lining side chains are important for anion specificity. However, while side chains are not conserved, the functional preservation of the anion selectivity sequence points to a shared mechanism between hCLC-Ka and other CLC channels and transporters.

The extensive hydrogen bonding network of permeating anions with pore-lining backbone amides (Fig. 1A–C) led us to hypothesize that backbone amides might provide the conserved pattern of anion coordination in the CLCs, while side chain interactions contribute to fine-tuning of ion selectivity. Using a combination of atomic mutagenesis, electrophysiology, and molecular dynamics (MD) simulations we show here that anion selectivity in CLC-0 and bCLC-k is determined by pore-lining backbone amides and their replacement with an ester oxygen destabilizes Cl^- binding with parallel effects on ion selectivity and permeation. Our results suggest that the role of backbone amides in ion selectivity depends on the side chain at the ‘gating glutamate’ position. Taken together, our results shed new light onto the mechanism of anion permeation and selectivity in a CLC channel and show that backbone amides are critical in allowing these channels to specifically select Cl^- over other anions.

Results

C-D loop orientation does not determine the role of Ser_{cen} in anion selectivity

We tested whether the structural arrangement of the C-D loop (Fig. 1A–C) determines the role of Ser_{cen} in CLC selectivity by replacing this residue with a proline in CLC-0, CLC-1 and bCLC-k (Fig. 1D–G, Supplementary Figs. 2, 3, 5, Supplementary Table 1). Consistent with past results, the anion selectivity of CLC-0 is drastically altered by the S123P mutation, with the mutant becoming more permeable to Br^- and NO_3^- than Cl^- (Fig. 1D, G, Supplementary Fig. 2, 3, 5, Supplementary Table 1)^{19,21}. However, absent direct structural information on this channel it is difficult to interpret this effect. Thus, we introduced the corresponding mutation in the structurally known bCLC-k and hCLC-1 channels that differ in the orientation of Ser_{cen} (Fig. 1B, C, E, F, Supplementary Figs. 2, 3, 5, Supplementary Table 1)^{33–35}. Unlike S123P CLC-0, mutant constructs of bCLC-k and hCLC-1 retain the selectivity sequences of their parent channels, $\text{Cl}^- > \text{Br}^- > \text{NO}_3^- > \text{I}^-$, with small alterations (Fig. 1G). While the lack of effect of the S121P mutant of bCLC-k could be rationalized based on the different orientation of the C-D loop in this channel, the lack of effect of S189P in hCLC-1 is more surprising. The wider intracellular constriction in CLC-1 could weaken binding to S_{cen}, as suggested by the lack of density at this site in the cryo-EM structure (Fig. 1C)^{34,35}. Alternatively, the C-D loop could interchange between the conformations seen in CLC-1 and bCLC-k, so that the importance of the hydrogen bond between an ion in S_{cen} and Ser_{cen} could depend on the stability of the two states. These results suggest other structural elements might play a more important role in determining the conserved selectivity sequence in CLCs.

Backbone amides contribute to anion selectivity in bCLC-k and CLC-0

To test the role of backbone amides in anion selectivity we used the nonsense suppression method to site-specifically replace amino acids whose backbone amides may participate in ion coordination with their α -hydroxy acid equivalents^{54,55}. This atomic manipulation ‘mutates’ the peptide bond into an ester bond by substituting the backbone NH group with an oxygen atom (Fig. 2A), thus eliminating the backbone’s ability to function as an H-bond donor, without altering side chain properties. The introduced ester is an otherwise modest change that shares similar bond lengths, angles, preference for a trans geometry, and comparably high energy barrier for rotation^{55,56}. We chose the bCLC-k and CLC-0 channels as representatives CLC channels where Ser_{cen} does not (bCLC-k) or does (CLC-0) control anion selectivity. Incorporation of the α -hydroxy acids at the tested positions in bCLC-k and CLC-0 results in robust currents with measurable shifts in reversal potentials in different anions (Supplementary Figs. 2–4). The ratio of the currents measured in oocytes injected with tRNA conjugated to the UAA or with unconjugated tRNA is >9 at all positions (Supplementary

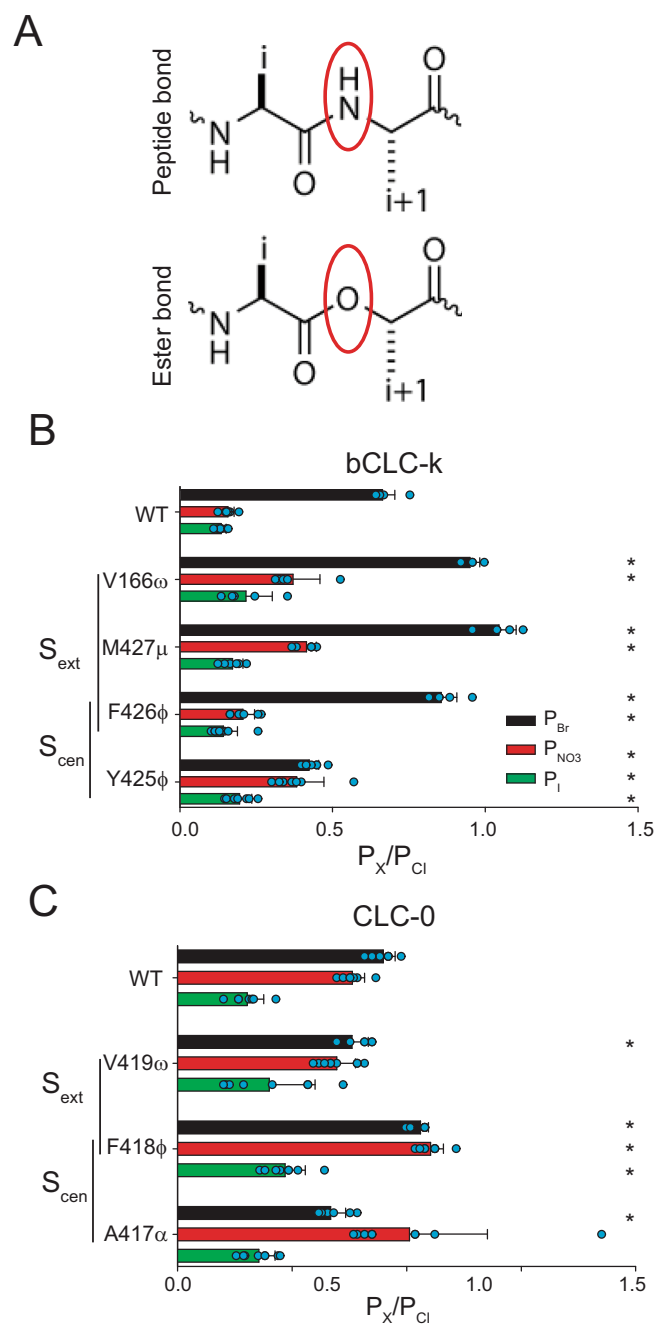


Fig. 2 | Role of backbone amides in anion selectivity of CLC-0 and bCLC-k.

A Schematic representation of peptide (top panel) and ester bonds (bottom panel). **(B, C)** Effect of replacing backbone amides with ester oxygens at positions lining S_{ext} and S_{cen} in bCLC-k **(B)** and CLC-0 **(C)** on P_{Br} (black bars), P_{NO_3} (red bars) and P_{I} (green bars). Nomenclature of α -hydroxy acid substitutions is explained in Methods. Data are Mean \pm St.Dev. of $n > 4$ repeats from $N \geq 3$ independent oocyte batches, individual data points are shown as cyan circles. The statistical significance of the effects of the mutants on the permeability ratios of each ion (indicated by *) was evaluated with a one-sided Student’s *t*-test with a Bonferroni correction (see “Methods”). Mean values and *p* values are reported in Supplementary Table 1. Individual data points are shown grouped by ion in Supplementary Fig. 5. Raw data for **B, C** is included in the Source Data Files.

Fig. 4A), suggesting that the contribution of currents due to non-specific incorporation and endogenous channels is $\leq 10\%$. The α -hydroxy acids for glycine or glutamate are not commercially available, and α -hydroxy substitutions in hCLC-1 did not yield sufficient currents for reversal potential determination.

In the bCLC-k channel, S_{ext} is lined by backbone amides of V166, M427 and F426, with F426 also lining S_{cen} together with Y425 (Fig. 1B). α -hydroxy substitutions at S_{ext} , V166 ω and M427 μ , result in an altered selectivity order of $\text{Br}^- > \text{Cl}^- > \text{NO}_3^- > \text{I}^-$ while the others retain the WT order (Fig. 2B). The effects on P_{Br} and P_{I} are relatively small, with <50% changes relative to the WT values (Supplementary Fig. 6B) while effects on P_{NO_3} are large at all positions, highlighted by a -250% P_{NO_3} increase in M427 μ (Supplementary Fig. 6B). Thus, backbone amides contribute to the overall selectivity of bCLC-k, and amides lining S_{ext} control the inter-anionic selectivity sequence.

We used the same approach to investigate the selectivity of the CLC-0 channel and found that mutating backbones lining S_{cen} results in altered selectivity sequences, with F418 ϕ not being able to discriminate between NO_3^- , Br^- and Cl^- , and A417 α showing an altered selectivity sequence of $\text{Cl}^- > \text{NO}_3^- > \text{Br}^- > \text{I}^-$ (Fig. 2C), while the S_{ext} -lining V419 ω substitution has a WT-like selectivity sequence (Fig. 2C). Thus, S_{cen} appears to primarily determine selectivity in CLC-0, consistent with previous results^{19,21,51}. Overall, the effects on P_{Br} , P_{NO_3} and P_{I} are relatively small, with <50% changes relative to the WT channel (Supplementary Fig. 6A), likely reflecting the weaker inter-anionic selectivity of CLC-0 compared to bCLC-k (Fig. 1G). In both channels, backbone substitutions have parallel effects on the permeability ratios and on the conductivity of the various ions, estimated from the ratio of the currents at +80 mV in the foreign anion to that of Cl^- (Supplementary Fig. 6C–H), indicating that interactions between backbone amides and the permeating ions determine binding and conduction.

Pore-lining backbone amides play key roles in CLC-0 gating

Backbone mutations in the pore affect the G - V relationships of the single-pore gating process of CLC-0 in Cl^- (Fig. 3A, Supplementary Fig. 7), with the A417 α substitution inducing a left shift in the G - V while

the F418 ϕ and V419 ω replacements cause a right-shift in $V_{1/2}$ (Fig. 3A, B). The direction of the $V_{1/2}$ shifts is preserved for all mutants in Br^- , NO_3^- and I^- , although the magnitudes vary (Fig. 3B). Correlation between the effects on selectivity and those on gating is poor, as the A417 α mutation strongly alters selectivity while having comparatively modest effects on gating and, conversely, the V419 ω replacement has a WT-like selectivity profile and the largest effects on the $V_{1/2}$. Remarkably, these mutations have dramatic effects on the common-pore gating process (Fig. 3C), with A417 α inverting its voltage dependence and V419 ω resulting in a nearly constitutive phenotype (Fig. 3D). Thus, removal of a single hydrogen-bonding group in the CLC-0 pore affects the global rearrangements associated with slow gating⁵⁷, supporting the idea of a strong allosteric coupling between local and global rearrangements in this channel^{46,47}.

Glu_{ex} modulates the role of backbone amides in selectivity

The differential roles of backbone amides in determining selectivity of CLC-0 and bCLC-k channels (Fig. 2) are surprising due to the overall structural conservation of CLC pores (Fig. 1). One obvious difference between these channels is that the highly conserved Glu_{ex} of CLC-0 (E166) is replaced by an uncharged valine in bCLC-k (V166) (Fig. 1B, Supplementary Fig. 1E). Introducing Glu_{ex} in the bCLC-k channel (V166E) or eliminating it from CLC-0 (E166A), has minor effects on selectivity with the V166E bCLC-k channel maintaining a WT-like sequence of $\text{Cl}^- > \text{Br}^- > \text{NO}_3^- > \text{I}^-$ (Fig. 4A), while the E166A CLC-0 mutant has a slightly altered sequence of $\text{Cl}^- > \text{Br}^- \geq \text{NO}_3^- > \text{I}^-$ (Fig. 4B).

We then introduced the backbone ester substitutions on the background of these mutants to test how Glu_{ex} modulates the role of backbone amides in selectivity. Currents mediated by the V166E/Y425 ϕ mutant were too small to obtain reliable results. The bCLC-k V166E/F426 ϕ mutant, however, displays a marked preference for Cl^- and does

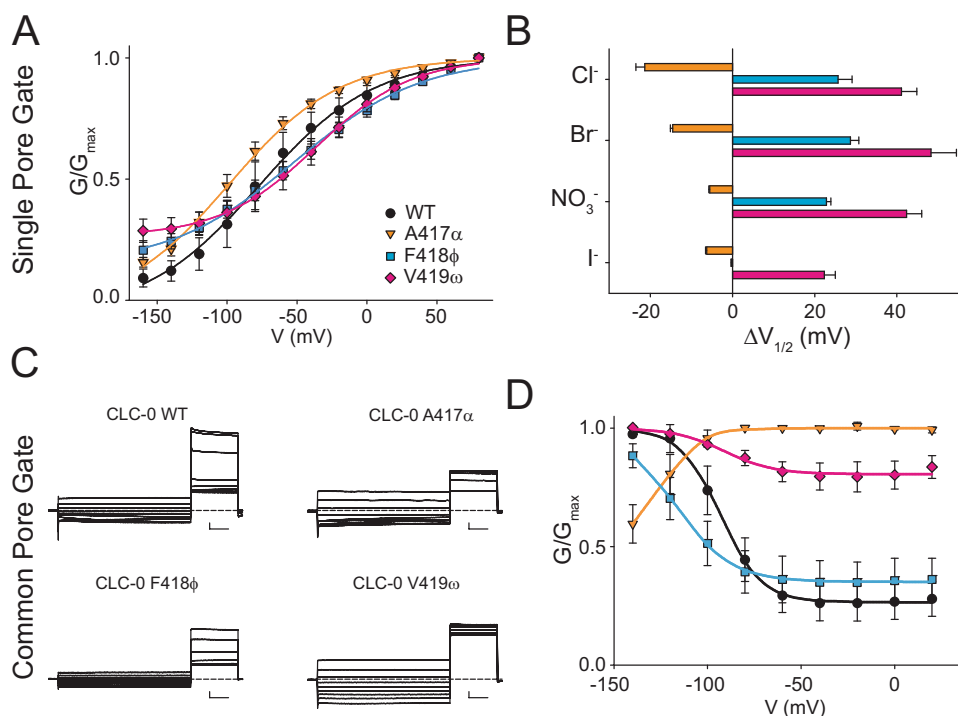


Fig. 3 | Pore-lining backbone amides affect fast and slow gating in CLC-0.

A Normalized G - V curves for fast gate of CLC-0 WT (black), A417 α (orange), F418 ϕ (cyan) and V419 ω (pink) in Cl^- . Solid lines are fits to Eq. 2. Values are mean \pm St. Dev. of $n > 7$ repeats from $N \geq 3$ independent oocyte batches. **B** $\Delta V_{1/2} = (V_{1/2}^{\text{mut}} - V_{1/2}^{\text{WT}})$ of the normalized fast gate G - V of WT and mutant CLC-0 in Cl^- , Br^- , NO_3^- and I^- . Colors as in **A**. Errors represent the propagation of the uncertainty of the $V_{1/2}$ parameter

evaluated from the fits of the data in **A** and Supplementary Fig. 7. **C** Representative slow gate current traces of WT and mutant CLC-0. Scale bars indicate 0.5 μA and 1 s. **D** Normalized G - V curves for slow gate of CLC-0 WT (black), A417 α (red), F418 ϕ (green) and V419 ω (yellow) in Cl^- . Solid lines are fits to Eq. 2. Values are mean \pm St. Dev. of $n > 7$ repeats from $N \geq 3$ independent oocyte batches. Raw data for **A**–**D** is included in the Source Data Files.

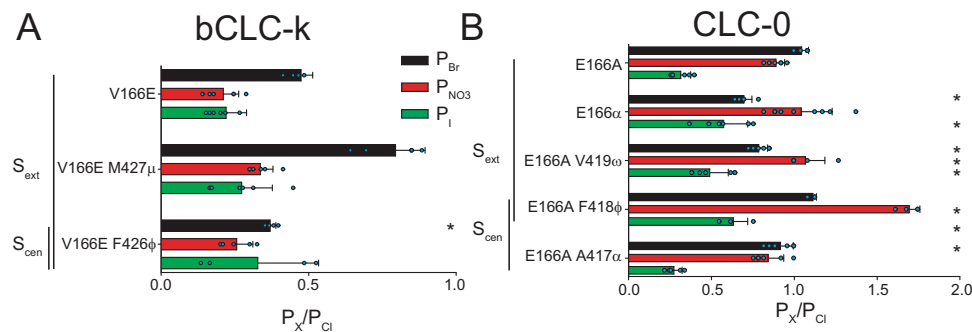


Fig. 4 | A glutamate side chain at the Glu_{ex} position modulates the role of S_{cen} and S_{ext} in anion selectivity. **A, B** Effect of replacing backbone amides with ester oxygens lining the S_{ext} and S_{cen} sites in V166E bCLC-k (**A**) and E166A CLC-0 (**B**) on P_{Br} (black bars), P_{NO₃} (red bars) and P_I (green bars). Data are Mean ± St.Dev. of $n > 4$ repeats from $N \geq 3$ independent oocyte batches, individual data points are shown as cyan circles. The statistical significance of the effects of the mutants on the

permeability ratios of each ion (indicated by *) was evaluated with a one-sided Student's *t*-test with a Bonferroni correction (see “Methods”). Mean values and *p* values are reported in Supplementary Table 1. Individual data points are shown grouped by ion in Supplementary Fig. 5. Raw data for **A, B** is included in the Source Data Files.

not discriminate among other anions resulting in an altered selectivity sequence of Cl⁻>Br⁻>I⁻>NO₃⁻ (Fig. 4A). In contrast, the V166E/M427μ mutant restores a WT-like selectivity sequence of Cl⁻>Br⁻>NO₃⁻>I⁻ (Fig. 4A), which was altered in the single M427μ mutant (Fig. 2B). In E166A CLC-0, the S_{ext}-lining E166α and E166A/V419ω substitutions have an altered selectivity sequence of NO₃⁻>Cl⁻>Br⁻>I⁻, suggesting an increased role for S_{ext} in anion selectivity (Fig. 4B). Conversely, the S_{cen}-lining E166A/A417α mutant restores a WT-like selectivity sequence (Fig. 4B) that was lost in the single A417α mutant (Fig. 2C). Most strikingly, the E166A/F418φ mutation converts CLC-0 into a NO₃⁻-selective channel with a selectivity sequence of NO₃⁻>>Br⁻>Cl⁻>I⁻ (Fig. 4B, Supplementary Fig. 6).

Overall, backbone manipulations in the absence of Glu_{ex} have larger relative effects on ion selectivity than those in the presence of Glu_{ex}, in particular for P_{NO₃} (Supplementary Fig. 6A, B). In both channels, there is an imperfect correlation between the presence of a protonatable side chain at position 166 and the roles of amides lining S_{cen} or S_{ext} (Supplementary Fig. 6A, B). Together these observations suggest that the selectivity of CLC pores is modulated by the presence of a glutamate side chain that competes with permeant anions for occupancy of S_{cen} and/or S_{ext}.

Role of backbone amides in stabilizing anions in the bCLC-k pore

To investigate the contribution of the protein residues, particularly the backbone amides, to stabilization of anions within the pore at a microscopic level, we simulated translocation of Cl⁻, Br⁻, I⁻, or NO₃⁻ through WT or M427μ bCLC-k channels³³ and calculated the potential of mean force (PMF) profiles associated with these single-ion permeation processes. For all anions, the PMF profiles show multiple local minima along the pore reporting on low-energy states of the ion where it establishes favorable interactions with the protein and local water molecules. Given the differences in sizes and H-bonding patterns of the anions (Fig. 5), small variations in the depth (-1–2 kcal/mole) and the exact positions (-1 Å) of these minima are observed.

The PMFs of WT channels show a global free energy minimum at S_{ext} for all four inspected anions (marked with a green dashed line in Fig. 5A), highlighting this site as the most stable anion-binding region along the pore. At this site the anions are mainly coordinated by the backbone amides of K165, V166, and M427. Among other minima, which are all significantly shallower than S_{ext}, noticeable are the one at or around S_{cen} (marked with a purple dashed line in Fig. 5A) in which the anions are coordinated by the backbone amide of Y425, and one in between S_{ext} and S_{cen} (marked with an orange dashed line in Fig. 5A) where the anions are coordinated by the backbone amides of G167 and Y425. These results indicate that the backbone amide interactions play

a key role in stabilizing the anions in all three minima (Fig. 5C). At all three sites, direct interactions between the anions and water molecules contributes to their stabilization. The M427μ replacement disrupts anion binding to S_{ext} (Fig. 5B) resulting in significant reduction of the well depth at this site or its complete disappearance as ions lose their favorable coordination with the amide hydrogen. Beyond local effects on S_{ext}, this mutation also affects the pattern of hydration, not only inside the constricted region, but also in the region between S_{ext} and S_{cen}, by altering the orientation of the water molecule coordinating to M427 in the WT protein (Fig. 5D). Furthermore, coordination analysis on the permeant anions suggests that the M427μ mutation affects the hydration and ion-protein interaction patterns beyond the S_{ext} site (Supplementary Fig. 8), which we believe could account for the PMF changes observed in other regions of the pore after the mutation. Previous MD studies showed that hydration and protein coordination of ions along the pore can affect the energetics of the ion permeation process in other channels^{58,59}. These results exemplify the critical contribution of backbone amide coordination for the anions within the pore. While this treatment does not represent the prevailing multi-ion permeation mechanism in these channels, it probes the environment of the anions in the pore and provides a reliable approximation for the energetics experienced by them.

Discussion

Ion channels employ diverse molecular strategies to enable the rapid and selective passage of ions across biological membranes. While cation selectivity is relatively well understood, the molecular bases of anion selectivity remain poorly characterized. Indeed, many anion channels are more permeable to non-physiological ions, such as I⁻ or SCN⁻, than to the physiologically abundant Cl⁻^{9–12,14} and most small-molecule compounds designed to bind and transport anions share a similarly poor selectivity profile^{60–62}, highlighting our limited understanding of the fundamental mechanisms of anion selectivity. Unique among anion channels, the CLCs specifically select for Cl⁻ over other anions. Past work suggested that the CLC preference for Cl⁻ is determined by the specific interactions with a pore-lining serine side chain on the C-D loop, as substitutions at this position confer selectivity for other anions^{19–21,23,50,52}. However, this mechanism was recently questioned as this loop adopts a different conformation in kidney-type CLC-k channels^{33,53} and its functional role is not conserved in the muscle-type CLC-I channel (Fig. 1G). Thus, the determinants of the conserved Cl⁻ selectivity of the CLCs remain unknown.

Ions in the CLC permeation pathway form hydrogen bonds with backbone amides lining S_{cen} and S_{ext}^{33,39} whose position is well-conserved among CLC proteins (Fig. 1, Supplementary Fig. 1). We used

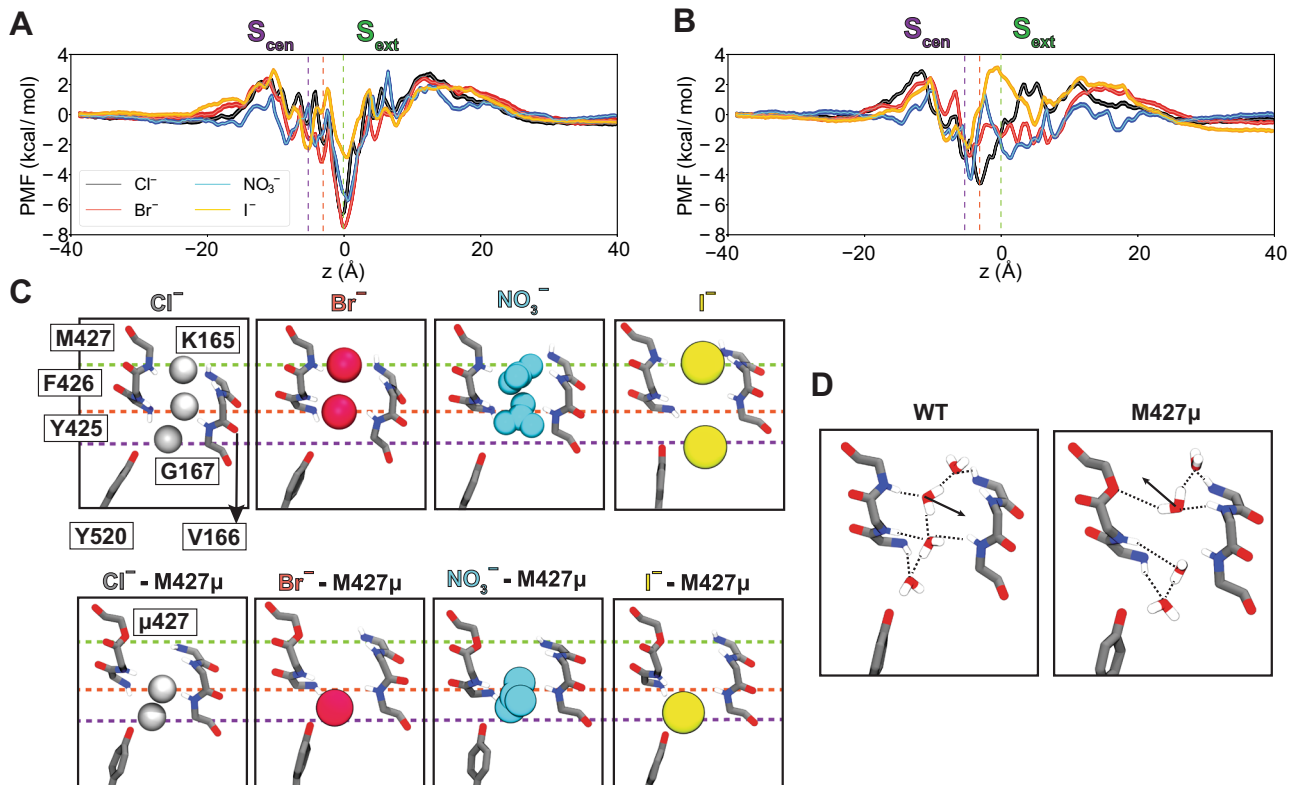


Fig. 5 | Anion-backbone interaction along the permeation pathway in WT and M427 μ bCLC-k. **A** Single-occupancy PMF calculated along the ion permeation pathway for Cl⁻, Br⁻, I⁻, and NO₃⁻ in WT bCLC-k. The z positions for the ions are specified relative to S_{ext} (z = 0). The positions of S_{ext}, an intermediate binding region, and S_{cen} are indicated by the green, orange, and purple vertical dashed lines, respectively. PMFs are aligned by their energy in the bulk solution. **B** Single-occupancy PMF calculated along the ion permeation pathway for Cl⁻, Br⁻, I⁻, and NO₃⁻ in the M427 μ mutant of bCLC-k. The uncertainty error in **(A)** and **(B)** is

calculated based on Monte Carlo bootstrapping and shown in shaded colors (almost unnoticeable). **C** The selectivity filter of bCLC-k along with the positions of all major binding sites (based on the PMFs, panels **(A)** and **(B)**) for different anions depicted in vdW for both WT and the M427 μ mutant (Cl⁻ in white, Br⁻ in red, NO₃⁻ in blue, and I⁻ in yellow). The three dashed lines correspond to those drawn in panels **(A)** and **(B)**. **D** Comparison of hydration patterns in the selectivity filter of WT and M427 μ bCLC-k, highlighting the shift in the orientations of water molecules.

atomic mutagenesis to site-specifically replace these putative hydrogen-bond donor, backbone amides with an ester oxygen that cannot engage in hydrogen bonds with the permeating anions^{55,56}. We found that targeted removal of individual pore-lining amides substantially degrades inter-anionic discrimination in both CLC-0 and bCLC-k, resulting in channels with weakened Cl⁻ preference (Figs. 2 and 4). Indeed, elimination of a single hydrogen bond within the selectivity filter can increase P_{NO₃} up to 250% and P_I up to 200% (Supplementary Fig. 6), while effects on P_{Br} are generally more modest, consistent with the idea that Br⁻ is a faithful substitute for Cl⁻^{31,38,43,48}. It is possible that the non-specific incorporation of amino acids and/or endogenous channels dampen the effects of backbone mutations on selectivity. However, currents recorded in oocytes injected with unconjugated tRNA are $\leq 10\%$ of those from tRNA conjugated to the α -hydroxy acids (Supplementary Fig. 4A), suggesting contributions of endogenous currents are relatively small and will not affect the observed trends. These errors could be higher for I⁻ currents, as this ion blocks CLCs but is more permeable through other Cl⁻ channels. Overall, the magnitude of the observed effects on selectivity is relatively small, likely reflecting the weaker interanion selectivity of Cl⁻ channels. Nonetheless, it is remarkable that single substitutions of single backbone atoms can alter the anion selectivity sequences of both bCLC-k and CLC-0 (Figs. 2 and 4). Notably, equivalent manipulations do not affect the selectivity sequence of K⁺ channels^{63,64}, supporting the idea that interactions between backbone amides and permeating anions are specifically important for selectivity in CLCs.

The specific roles of backbone amides depend on the specific channel environment, as equivalent substitutions do have the same effects in CLC-0 and bCLC-k (Fig. 2). Further, not all backbone amides play comparable roles in selectivity, for example V166 ω and M427 μ render bCLC-k less selective whereas F426 ϕ increases its preference for Cl⁻ (Fig. 2). These differences could arise, at least in part, from contributions of variable pore-lining side chains. Indeed, the roles of backbone amides in anion selectivity is enhanced in channel constructs lacking a Glu_{ex} side chain (E166A CLC-0 and WT bCLC-k) relative to those with a glutamate at this position (WT CLC-0 and V166E bCLC-k) (Figs. 2, 4, Supplementary Fig. 6), and side chains also play roles in selectivity in some CLCs (Fig. 1)^{19–21,23,51,53}. Thus, we propose that Cl⁻ specificity in CLC channels and transporters arises from the combined contributions of pore-lining backbone amides and side chains. Together, our data suggests that the structurally conserved orientation of backbone amides provides optimized coordination for the permeating Cl⁻ ions while pore-lining side chains, that are variable in sequence and orientation, modulate the contributions of individual backbone amides as well as directly coordinating ions in the pore, as suggested by the poorly conserved role of the Ser_{cen} side chain in CLC selectivity. Further work is required to dissect the contributions of individual structural elements to anion selectivity.

It is important to consider that ion permeation through the CLCs is a multi-ion process⁴⁶, which raises the possibility that ion selectivity could also be determined by multi-ion occupancy of the pore. However, several lines of evidence suggest this is not the case. First, the CLC channels and exchangers share the same selectivity sequence despite

having different mechanisms of ion transport. Second, in CLC-ec1 – a CLC transporter that shares the same ion selectivity as the CLC-0 and bCLC-k channels studied here – the selectivity of ion binding and transport coincide^{18,19} and ion binding to the different sites is largely unaffected in single or multi-ion configurations^{19,38}. Together, these observations suggest that the selectivity properties of the CLC Cl⁻ permeation pathway are determined by the interactions of single ions with the pore and thus can be evaluated using single-ion PMF calculations (Fig. 5). Our free energy calculations highlight the involvement of backbone-ion coordination in the stabilization of the ions in the channel's selectivity filter and at the S_{ext} site, where we find that mutating the pore-lining backbone amide of M427 μ directly and significantly destabilizes ion binding. Notably, our simulations show this manipulation also results in longer-range effects as it perturbs the hydration pattern of the pore (Fig. 5D). Finally, we found that substituting pore-lining backbone amides affects CLC-0 gating, with particularly marked effects on common gate activation. This supports the idea of tight allosteric coupling between ions permeating through the pore and the local and the global rearrangements that respectively underlie single- and common-pore gating processes in this channel^{46,47}.

Our MD simulations suggest that in CLC-k the ions are most strongly bound at the S_{ext} site. In the backbone mutant M427 μ , S_{ext} becomes unstable and the binding positions of ions and water near S_{cen} are shifted down with a clear change in their orientations, factors that likely result in the channel's loss of selectivity for Cl⁻. The proposed mechanism, that ion selectivity is primarily determined via interactions with backbone elements, is reminiscent of the mechanism for selectivity in K⁺ channels^{1,2}. The channel's structure is optimized to provide an ideal coordination shell to the permeating ion via interaction with its backbone, where the choice of carbonyls or amides facilitates ions of different charge.

Methods

In vitro cRNA transcription

RNAs for all CLC-0 and bCLC-k wild-type and mutant constructs were transcribed from a pTLN vector using the mMessage mMachine SP6 Kit (Thermo Fisher Scientific, Grand Island, NY)^{46,52,65}. For final purification of cRNA the RNeasy Mini Kit (Quiagen, Hilden, Germany) was employed. RNA concentrations were determined by absorbance measurements at 260 nm and quality was confirmed on a 1% agarose gel.

tRNA miscacylation

For nonsense suppression of CLC-0 and bCLC-k TAG mutants in *Xenopus laevis* oocytes, THG73 and PylT tRNAs have been employed. THG73 was transcribed, folded and miscacylated as previously described⁶⁶. PylT was synthesized by Integrated DNA Technologies, Inc. (Coralville, IA, USA), folded and miscacylated as previously described⁶⁷. Ala-, Met-, Phe-, Val-, α -hydroxy Ala- (α), α -hydroxy Met- (μ), α -hydroxy Phe- (φ) and α -hydroxy Val-pdCpA (ω) substrates were synthesized according to published procedures⁶⁷.

Nonsense suppression to replace amino acids with α -hydroxy acid

The nonsense suppression method was used to site-specifically replace amino acids with pore-lining backbone amides with their α -hydroxy acid equivalents⁵⁵. This atomic manipulation substitutes the backbone NH group with an oxygen atom, eliminating the ability of the backbone to function as H-bond donor without altering side chain properties (Fig. 2A), converting the peptide bond into an ester bond. These bonds have similar lengths, angles, preference for a trans geometry, and comparably high energy barrier for rotation^{55,56}. Incorporation of the α -hydroxy acids at the positions tested in bCLC-k (V166, Y425, F426, M427) and CLC-0 (E166, A417, F418, V419) resulted in currents that were at least 9-fold higher than those recorded in oocytes injected with non-

acetylated control tRNA (Supplementary Fig. 4A). We indicate mutations to α -hydroxy acids with their Greek letter counterpart: α for α -hydroxy alanine, ω for α -hydroxy valine, φ for α -hydroxy phenylalanine and μ α -hydroxy methionine. Incorporation of WT amino acids resulted in channels with WT-like properties (Supplementary Fig. 4B, C). Finally, insertion of φ at position F161 (F161 φ) in CLC-0, a pore-lining residue located near Glu_{ex} (E166) but not involved in ion binding, resulted in WT-like selectivity (Supplementary Fig. 4D, E). These results indicate that effects on selectivity specifically reflect the incorporation of α -hydroxy acids at the targeted positions.

We were not able to test the role of the following residues: (i) G164 (bCLC-k and CLC-0) because the α -hydroxy glycine acylated to the suppressor tRNA was very prone to hydrolysis impeding the incorporation; (ii) K165 (bCLC-k), R165 (CLC-0), and E166 as α -hydroxy acids could not be synthesized, and (iii) we used α -hydroxy phenylalanine (φ) at position Y425 (bCLC-k) as the incorporation of α -hydroxy tyrosine was not successful. Phenylalanine was used as control in this case (Supplementary Fig. 4B). Currents associated with the V166E Y425 φ mutant were too small to be analyzable. The nonsense suppression approach did not result in analyzable currents of CLC-1, CLC-5 or CLC-7.

Protein expression in *Xenopus laevis* oocytes and two electrode voltage clamp (TEVC) recordings

Xenopus laevis oocytes were purchased from Ecocyte Bio Science (Austin, TX, USA) and Xenocyte (Dexter, Michigan, USA) or kindly provided by Dr. Pablo Artigas (Texas Tech University, USA, protocol # 11024). For conventional CLC expression, the following injection and expression conditions have been used: for CLC-0, 0.1–5 ng cRNA were injected and currents were measured –6–24 h after injection; for CLC-1, –2 ng cRNA were injected and currents were measured ~ 24 h after injection; –0.1 ng of each, CLC-K and Barttin cRNA, were coinjected and currents were measured the day after injection. For nonsense suppression of CLC-0 and bCLC-k constructs, cRNA and miscacylated tRNA were coinjected (up to 25 ng of cRNA and up to 250 ng of tRNA per oocyte) and currents were recorded 6–24 h after injection.

TEVC was performed as described^{19,68}. In brief, voltage-clamped chloride currents were recorded in ND96 solution (in mM: 96 NaCl, 2 KCl, 1.8 CaCl₂, 1 MgCl₂, 5 HEPES, pH 7.5) using an OC-725C voltage clamp amplifier (Warner Instruments, Hamden, CT). Ion substitution experiments were performed by replacing the 96 mM NaCl in the external solution with equimolar amounts of NaBr, NaNO₃ or NaI. Data was acquired with Patchmaster (HEKA Elektronik, Lambrecht, Germany) at 5 kHz and filtered with Frequency Devices 8-pole Bessel filter at a corner frequency of 2 kHz. Analysis was performed using Ana (M. Pusch, Istituto di Biofisica, Genova), Sigmaplot (SPSS Inc.) and Prism (GraphPad, San Diego, CA, USA). For each substitution we recorded currents from oocytes injected with unconjugated tRNA (Fig. 3 Supplementary 1A). This current, I(tRNA), reflects a combination of the contributions of CLC channels with non-specific incorporation of conventional amino acids and of the endogenous currents. In all cases, the ratio of the currents measured in oocytes injected with tRNA conjugated to the UAA, I(UAA), to I(tRNA) is >9 (Fig. 3 Supplementary 1A). This suggests that the contribution of currents due to non-specific incorporation and endogenous channels is $\leq 10\%$ and thus will not affect the trends of the observed effects. It is possible that the contribution to error could be higher for I⁻ currents, as this ion blocks CLCs but is more permeable through other Cl⁻ channels.

Oocytes were held at a resting potential of –30 mV. For CLC-0 two different recording protocols have been used to distinguish single-pore from common-pore gating. During the single-pore gating protocol the voltage was stepped to +80 mV for 50 ms and then a variable voltage from –160 mV to +80 mV increasing in 20 mV steps was applied for 200 ms, followed by a 50 ms pulse at –120 mV for tail current analysis. For CLC-0 common-pore gating, 7 s voltage steps

from +20 mV to -140 mV have been applied in -20 mV increments followed by a 2.5 s +60 mV post pulse for tail current analysis. For bCLC-k the voltage was stepped to -30 mV for 20 ms and then a variable voltage from -80 mV to +80 mV increasing in 10 mV steps was applied for 150 ms, followed by a 20 ms pulse at -30 mV. For CLC-1 the voltage was stepped to +80 mV for 100 ms and then a variable voltage from -160 mV to +80 mV increasing in 20 mV steps was applied for 200 ms, followed by a 100 ms pulse at -100 mV for tail current analysis.

Analysis of electrophysiological recordings

Permeability ratios were determined by measuring the change in reversal potential, ΔV_{rev} , recorded upon substituting the external anion and using the Goldman-Hodgkin-Katz equation¹⁵ as

$$\Delta V_{\text{rev}} = \left(V_{\text{rev}}^2 - V_{\text{rev}}^1 \right) = \left(\frac{RT}{zF} \ln \frac{P_{\text{Cl}}[\text{Cl}]_{\text{ex}}^2 + P_{\text{X}}[\text{X}]_{\text{ex}}^2}{P_{\text{Cl}}[\text{Cl}]_{\text{in}}} \right) - \left(\frac{RT}{zF} \ln \frac{P_{\text{Cl}}[\text{Cl}]_{\text{ex}}^1}{P_{\text{Cl}}[\text{Cl}]_{\text{in}}} \right) = \frac{RT}{zF} \ln \frac{P_{\text{Cl}}[\text{Cl}]_{\text{ex}}^2 + P_{\text{X}}[\text{X}]_{\text{ex}}^2}{P_{\text{Cl}}[\text{Cl}]_{\text{ex}}^1} \quad (1)$$

Where R , T , F and z have the usual meaning. The assumption that $[\text{Cl}]_{\text{in}}$ did not change during successive perfusions was validated by bracketing recordings in Br^- and NO_3^- with a return measurement in external Cl^- and ensuring that V_{rev} did not shift by more than 3 mV. Thus, the sequence of experiments was Cl^- (1), Br^- , Cl^- (2), NO_3^- , Cl^- (3), Γ (Supplementary Fig. 3). In some cases, the order of Br^- and NO_3^- was inverted, but no differences were detected. Γ was kept as the last ion tested due to its slow washout from oocytes. To simplify notation, throughout the text we indicate the relative permeability ratios of Br^- , NO_3^- , and Γ as P_{Br} , P_{NO_3} and P_{Γ} with the understanding that these values represent the relative permeability ratios of these anions to that of Cl^- , $P_{\text{Br, NO}_3, \Gamma}/P_{\text{Cl}}$.

To estimate the voltage dependence of WT and mutant CLC-0, tail current analysis was performed, and data was fit to a Boltzmann function of the form:

$$P_o = P_{\text{min}} + \frac{(1 - P_{\text{min}})}{1 + e^{(V_{0.5} - V)/k}} \quad (2)$$

where P_o is the open probability as a function of voltage and is assumed to reach a value of unity at full activation. P_{min} is the residual open probability independent of voltage. $V_{0.5}$ is the voltage at which 50% activation occurs, and $k = RT/zF$ is the slope factor, R is the universal gas constant, T is temperature in K , F is the Faraday constant, and z is the gating charge.

Statistical analysis

All values are presented as mean \pm S.Dev. as indicated in the pertinent figure legends. One-sided Student's t -test was performed to determine statistical significance of effects. We compared the effects of each α -hydroxy substitution to its parent construct. Thus, each single mutant was compared to the WT channel constructs whereas each double mutant was compared to the corresponding E166A or V166E mutants. The threshold for significance of the one-sided Student's t -test was assigned using a threshold of $p = 0.05$ and a Bonferroni correction. Thus, the significance thresholds are: CLC-0 WT $p < 0.007$, CLC-0 E166A $p < 0.006$; bCLC-k WT $p < 0.0055$; bCLC-k V166E $p < 0.01$ and CLC-1 $p < 0.05$.

Statistics and reproducibility

Functional experiments were repeated 4+ times from 3+ independent oocyte batches.

Simulation systems setup

For the bovine bCLC-k channel, the cryo-EM structures³³ (pdb:5TQQ) were used as the structural model for all the MD simulations and free energy calculations. Two unstructured loop regions missing in the cryo-EM structures (residue 258-276 and 454-456) were modeled using SuperLooper⁶⁹. The resulting models were embedded in lipid bilayers consisting of 80% POPC and 20% cholesterol and solvated with 0.15 M of NaCl and TIP3P water⁷⁰ using CHARMM-GUI MEMBRANE BUILDER⁷¹. The dimension for the simulated systems was $150 \times 150 \times 130 \text{ \AA}^3$.

The simulation system was energy-minimized for 10,000 steps, followed by two steps of 1-ns relaxation. The simulation system was then subjected to 1 ns of NPT initial equilibration with the standard protocol described in the CHARMM-GUI MEMBRANE BUILDER, which involves gradually releasing positional and dihedral restraints on the protein and lipid molecules. Thereafter, 10 ns of NPT equilibration with dihedral restraints ($k = 100 \text{ kcal/mol/rad}^2$) on the protein secondary structure were performed. After equilibration, the simulation system was equilibrated for another 250 ns without any restraints. This equilibrated system was used for all the free energy calculations.

Simulation protocols

All simulations were carried out with NAMD 2.13^{72,73}, using CHARMM36m protein⁷⁴ and CHARMM36 lipid⁷⁵ parameters. The SHAKE algorithm⁷⁶ was employed to constrain bonds involving hydrogens to allow 2-fs timesteps for the integrator. A constant temperature of 310 K was maintained by Langevin thermostat⁷⁷ with a damping coefficient of 1 ps^{-1} . Nosé-Hoover Langevin piston⁷⁸ with a period of 200 ps and a decay time of 50 ps was employed to maintain constant pressure at 1 atm. Periodic boundary conditions and a non-bonded cutoff of 12 Å (with a 10 Å switching distance and using vdW force switching) were used. Long-range electrostatics were calculated using the particle mesh Ewald method⁷⁹ with 1-Å grid spacing. Bonded interactions and short-range nonbonded interactions were calculated every timestep (2 fs). The pairs of atoms whose interactions were evaluated (neighborhood list) were updated every 20 fs. A cutoff (13.5 Å) slightly longer than the nonbonded cutoff was applied to search for interacting atom pairs. Publicly available software package VMD was used for the analysis and visualization of the molecular system (<https://www.ks.uiuc.edu/Research/vmd/>).

Free energy calculations

The free energy profiles, or the potential of mean force (PMF), of ion translocation through the permeation pore of bCLC-k were calculated using an enhanced sampling technique, umbrella sampling (US)⁸⁰. In the US simulations, the reaction coordinate was chosen to be the z position (along the membrane normal) of the restrained ion relative to S_{ext} (set to $z = 0$), as the permeation pathway near the selectivity filter is roughly parallel to the membrane normal (aligned with the z -axis). To restrain the ion movement through the selectivity filter, the xy coordinates of the ion were confined by a cylindrical half-harmonic wall ($k = 10 \text{ kcal/mol/\AA}^2$) with a radius of 30 Å centering around the axis of the permeation pathway. For each ion the conduction pathway was divided into 80 umbrella windows with 1 Å interval and ranging from $z = -40 \text{ \AA}$ to $z = 40 \text{ \AA}$, assuring the ion was in solution at each end. In each window, the ion was harmonically restrained along the reaction coordinate ($k = 5 \text{ kcal/mol/\AA}^2$), and initially equilibrated for 1 ns. Production sampling over each window was then done for 10 ns. The obtained distributions were then unbiased and combined using the weighted histogram analysis method (WHAM)⁸¹ to obtain the PMF of the ion movement along the pore axis. The convergence of each PMF was examined by constructing the PMF after 5 to 10 ns of sampling with 1 ns interval. All the obtained PMFs remain unchanged after 9 ns of sampling, indicating a good degree of convergence (Fig. 5 Sup. 2). The final PMFs are constructed with 10 ns of sampling and uncertainty errors are calculated based on Monte Carlo bootstrapping.

Reporting summary

Further information on research design is available in the Nature Portfolio Reporting Summary linked to this article.

Data availability

All data, constructs and electrophysiological traces are available on request. MD simulation files are available at: <https://doi.org/10.5281/zenodo.7317338>. Source data are provided with this paper.

References

- Doyle, D. A. et al. The structure of the potassium channel: molecular basis of K⁺ conduction and selectivity. *Science* **280**, 69–77 (1998).
- Zhou, Y., Morais-Cabral, J. H., Kaufman, A. & MacKinnon, R. Chemistry of ion coordination and hydration revealed by a K⁺ channel-Fab complex at 2.0 Å resolution. *Nature* **414**, 43–48 (2001).
- Morais-Cabral, J. H., Zhou, Y. & MacKinnon, R. Energetic optimization of ion conduction rate by the K⁺ selectivity filter. *Nature* **414**, 37–42 (2001).
- Noskov, S. Y., Bernèche, S. & Roux, B. Control of ion selectivity in potassium channels by electrostatic and dynamic properties of carbonyl ligands. *Nature* **431**, 830–834 (2004).
- Lockless, S. W., Zhou, M. & MacKinnon, R. Structural and thermodynamic properties of selective ion binding in a K⁺ channel. *PLoS Biol.* **5**, e121 (2007).
- Thompson, A. et al. Mechanism of potassium-channel selectivity revealed by Na⁺ and Li⁺ binding sites within the KcsA pore. *Nat. Struct. Mol. Biol.* **16**, 1317–1324 (2009).
- Payandeh, J., Scheuer, T., Zheng, N. & Catterall, W. A. The crystal structure of a voltage-gated sodium channel. *Nature* **475**, 353 (2011).
- Tang, L. et al. Structural basis for Ca²⁺ selectivity of a voltage-gated calcium channel. *Nature* **505**, 56 (2013).
- Bormann, J., Hamill, O. P. & Sakmann, B. Mechanism of anion permeation through channels gated by glycine and gamma-aminobutyric acid in mouse cultured spinal neurones. *J. Physiol.* **385**, 243–286 (1987).
- Hwang, T.-C. & Kirk, K. L. The CFTR ion channel: gating, regulation, and anion permeation. *Cold Spring Harb. Perspect. Med.* **3**, a009498–a009498 (2013).
- Ni, Y.-L., Kuan, A.-S. & Chen, T.-Y. Activation and inhibition of TMEM16A calcium-activated chloride channels. *PLoS ONE* **9**, e86734 (2014).
- Pifferi, S. Permeation mechanisms in the TMEM16B calcium-activated chloride channels. *PLoS ONE* **12**, e0169572 (2017).
- Vaisey, G., Miller, A. N. & Long, S. B. Distinct regions that control ion selectivity and calcium-dependent activation in the bestrophin ion channel. *Proc. Natl Acad. Sci. USA* **113**, E7399–E7408 (2016).
- Qu, Z. & Hartzell, C. Determinants of anion permeation in the second transmembrane domain of the mouse bestrophin-2 chloride channel. *J. Gen. Physiol.* **124**, 371–382 (2004).
- Hille, B. *Ion Channels of Excitable Membranes*, 3rd edn (Sinauer, 2001).
- Fahlke, C., Dürr, C. & George, A. L. Jr Mechanism of ion permeation in skeletal muscle chloride channels. *J. Gen. Physiol.* **110**, 551–564 (1997).
- Rychkov, G. Y., Pusch, M., Roberts, M. L., Jentsch, T. J. & Bretag, A. H. Permeation and block of the skeletal muscle chloride channel, CLC-1, by foreign anions. *J. Gen. Physiol.* **111**, 653–665 (1998).
- Accardi, A., Kolmakova-Partensky, L., Williams, C. & Miller, C. Ionic currents mediated by a prokaryotic homologue of CLC Cl⁻ channels. *J. Gen. Physiol.* **123**, 109–119 (2004).
- Picollo, A., Malvezzi, M., Houtman, J. C. & Accardi, A. Basis of substrate binding and conservation of selectivity in the CLC family of channels and transporters. *Nat. Struct. Mol. Biol.* **16**, 1294–1301 (2009).
- Zifarelli, G. & Pusch, M. Conversion of the 2 Cl⁻/1 H⁺ antiporter CLC-5 in a NO₃⁻/H⁺ antiporter by a single point mutation. *EMBO J.* **10**, 1111–1116 (2009).
- Bergsdorf, E. Y., Zdebik, A. A. & Jentsch, T. J. Residues important for nitrate/proton coupling in plant and mammalian CLC transporters. *J. Biol. Chem.* **284**, 11184–11193 (2009).
- De Angeli, A. et al. The nitrate/proton antiporter AtCLCa mediates nitrate accumulation in plant vacuoles. *Nature* **442**, 939–942 (2006).
- Wege, S. et al. The proline 160 in the selectivity filter of the Arabidopsis NO₃⁻/H⁺ exchanger AtCLCa is essential for nitrate accumulation in planta. *Plant J.* **63**, 861–869 (2010).
- Brammer, A. E., Stockbridge, R. B. & Miller, C. F⁻/Cl⁻ selectivity in CLCF-type F⁻/H⁺ antiporters. *J. Gen. Physiol.* **144**, 129–136 (2014).
- Lim, H. H., Stockbridge, R. B. & Miller, C. Fluoride-dependent interruption of the transport cycle of a CLC Cl⁻/H⁺ antiporter. *Nat. Chem. Biol.* **9**, 712–715 (2013).
- Stockbridge, R. B. et al. Fluoride resistance and transport by riboswitch-controlled CLC antiporters. *Proc. Natl Acad. Sci. USA* **109**, 15289–15294 (2012).
- Last, N. B. et al. A CLC-type F⁻/H⁺ antiporter in ion-swapped conformations. *Nat. Struct. Mol. Biol.* **25**, 601–606 (2018).
- Jentsch, T. J. & Pusch, M. CLC chloride channels and transporters: structure, function, physiology, and disease. *Physiol. Rev.* **98**, 1493–1590 (2018).
- Accardi, A. Structure and gating of CLC channels and exchangers. *J. Physiol.* **593**, 4129–4138 (2015).
- Dutzler, R. The structural basis of CLC chloride channel function. *Trends Neurosci.* **27**, 315–320 (2004).
- Dutzler, R., Campbell, E. B. & MacKinnon, R. Gating the selectivity filter in CLC chloride channels. *Science* **300**, 108–112 (2003).
- Feng, L., Campbell, E. B., Hsiung, Y. & MacKinnon, R. Structure of a eukaryotic CLC transporter defines an intermediate state in the transport cycle. *Science* **330**, 635–641 (2010).
- Park, E., Campbell, E. B. & MacKinnon, R. Structure of a CLC chloride ion channel by cryo-electron microscopy. *Nature* **541**, 500–505 (2017).
- Park, E. & MacKinnon, R. Structure of the CLC-1 chloride channel from Homo sapiens. *eLife* **7**, e36629 (2018).
- Wang, K. et al. Structure of the human CLC-1 chloride channel. *PLoS Biol.* **17**, e3000218 (2019).
- Schrecker, M., Korobenko, J. & Hite, R. K. Cryo-EM structure of the lysosomal chloride-proton exchanger CLC-7 in complex with OSTM1. *eLife* **9**, e59555 (2020).
- Zhang, S. et al. Molecular insights into the human CLC-7/Ostm1 transporter. *Sci. Adv.* **6**, eabb4747 (2020).
- Lobet, S. & Dutzler, R. Ion-binding properties of the CLC chloride selectivity filter. *Embo J.* **25**, 24–33 (2006).
- Dutzler, R., Campbell, E. B., Cadene, M., Chait, B. T. & MacKinnon, R. X-ray structure of a CLC chloride channel at 3.0 Å reveals the molecular basis of anion selectivity. *Nature* **415**, 287–294 (2002).
- Accardi, A. & Miller, C. Secondary active transport mediated by a prokaryotic homologue of CLC Cl⁻ channels. *Nature* **427**, 803–807 (2004).
- Miller, C. CLC chloride channels viewed through a transporter lens. *Nature* **440**, 484–489 (2006).
- Feng, L., Campbell, E. B. & MacKinnon, R. Molecular mechanism of proton transport in CLC Cl⁻/H⁺ exchange transporters. *Proc. Natl Acad. Sci. USA* **109**, 11699–11704 (2012).
- Nguitragool, W. & Miller, C. Uncoupling of a CLC Cl⁻/H⁺ exchange transporter by polyatomic anions. *J. Mol. Biol.* **362**, 682–690 (2006).
- Alekov, A. K. & Fahlke, C. Channel-like slippage modes in the human anion/proton exchanger CLC-4. *J. Gen. Physiol.* **133**, 485–496 (2009).

45. Orhan, G., Fahlke, C. & Alekov, A. K. Anion- and proton-dependent gating of CLC-4 anion/proton transporter under uncoupling conditions. *Biophys. J.* **100**, 1233–1241 (2011).
46. Pusch, M., Ludewig, U., Rehfeldt, A. & Jentsch, T. J. Gating of the voltage-dependent chloride channel CLC-0 by the permeant anion. *Nature* **373**, 527–531 (1995).
47. Chen, T. Y. & Miller, C. Nonequilibrium gating and voltage dependence of the CLC-0 Cl⁻ channel. *J. Gen. Physiol.* **108**, 237–250 (1996).
48. Accardi, A., Lobet, S., Williams, C., Miller, C. & Dutzler, R. Synergism between halide binding and proton transport in a CLC-type exchanger. *J. Mol. Biol.* **362**, 691–699 (2006).
49. Walden, M. et al. Uncoupling and turnover in a Cl⁻/H⁺ exchange transporter. *J. Gen. Physiol.* **129**, 317–329 (2007).
50. Ludewig, U., Pusch, M. & Jentsch, T. J. Two physically distinct pores in the dimeric CLC-0 chloride channel. *Nature* **383**, 340–343 (1996).
51. Ludewig, U., Pusch, M. & Jentsch, T. J. Independent gating of single pores in CLC-0 chloride channels. *Biophys. J.* **73**, 789–797 (1997).
52. Leisle, L., Ludwig, C. F., Wagner, F. A., Jentsch, T. J. & Stauber, T. CLC-7 is a slowly voltage-gated 2Cl⁻/1H⁺-exchanger and requires Ostm1 for transport activity. *EMBO J.* **30**, 2140–2152 (2011).
53. Lagostena, L., Zifarelli, G. & Picollo, A. New insights into the mechanism of NO₃⁻ selectivity in the human kidney chloride channel CLC-Ka and the CLC protein family. *J. Am. Soc. Nephrol.* **30**, 293–302 (2019).
54. England, P. M., Zhang, Y., Dougherty, D. A. & Lester, H. A. Backbone mutations in transmembrane domains of a ligand-gated ion channel: implications for the mechanism of gating. *Cell* **96**, 89–98 (1999).
55. Sereikaitė, V. et al. Probing backbone hydrogen bonds in proteins by amide-to-ester mutations. *Chembiochem* **19**, 2136–2145 (2018).
56. Powers, E. T., Deechongkit, S. & Kelly, J. W. Backbone-backbone H-bonds make context-dependent contributions to protein folding kinetics and thermodynamics: lessons from amide-to-ester mutations. *Adv. Protein Chem.* **72**, 39–78 (2005).
57. Bykova, E. A., Zhang, X. D., Chen, T. Y. & Zheng, J. Large movement in the C terminus of CLC-0 chloride channel during slow gating. *Nat. Struct. Mol. Biol.* **13**, 1115–1119 (2006).
58. Richards, L. A., Schäfer, A. I., Richards, B. S. & Corry, B. The importance of dehydration in determining ion transport in narrow pores. *Small* **8**, 1701–1709 (2012).
59. Richards, L. A., Schäfer, A. I., Richards, B. S. & Corry, B. Quantifying barriers to monoanion anion transport in narrow non-polar pores. *Phys. Chem. Chem. Phys.* **14**, 11633–11638 (2012).
60. Wu, X. et al. Nonprotonophoric electrogenic Cl⁻ transport mediated by valinomycin-like carriers. *Chem* **1**, 127–146 (2016).
61. Hernando, E. et al. Small molecule anionophores promote transmembrane anion permeation matching CFTR activity. *Sci. Rep.* **8**, 2608 (2018).
62. Jentsch, A. V. et al. Transmembrane anion transport mediated by halogen-bond donors. *Nat. Commun.* **3**, 905 (2012).
63. Lu, T. et al. Probing ion permeation and gating in a K⁺ channel with backbone mutations in the selectivity filter. *Nat. Neurosci.* **4**, 239–246 (2001).
64. Valiyaveetil, F. I., Sekedat, M., MacKinnon, R. & Muir, T. W. Structural and functional consequences of an amide-to-ester substitution in the selectivity filter of a potassium channel. *J. Am. Chem. Soc.* **128**, 11591–11599 (2006).
65. Steinmeyer, K., Schwappach, B., Bens, M., Vandewalle, A. & Jentsch, T. J. Cloning and functional expression of rat CLC-5, a chloride channel related to kidney disease. *J. Biol. Chem.* **270**, 31172–31177 (1995).
66. Leisle, L. et al. Cellular encoding of Cy dyes for single-molecule imaging. *eLife* **5**, e19088 (2016).
67. Infield, D. T., Lueck, J. D., Galpin, J. D., Galles, G. D. & Ahern, C. A. Orthogonality of Pyrrolysine tRNA in the *Xenopus* oocyte. *Sci. Rep.* **8**, 5166–5166 (2018).
68. Leisle, L. et al. Divergent Cl⁻ and H⁺ pathways underlie transport coupling and gating in CLC exchangers and channels. *eLife* **9**, e51224 (2020).
69. Hildebrand, P. W. et al. SuperLooper—a prediction server for the modeling of loops in globular and membrane proteins. *Nucleic Acids Res.* **37**, W571–W574 (2009).
70. Jorgensen, W. L., Chandrasekhar, J., Madura, J. D., Impey, R. W. & Klein, M. L. Comparison of simple potential functions for simulating liquid water. *J. Chem. Phys.* **79**, 926–935 (1983).
71. Wu, E. L. et al. CHARMM-GUI Membrane Builder toward realistic biological membrane simulations. *J. Comput. Chem.* **35**, 1997–2004 (2014).
72. Phillips, J. C. et al. Scalable molecular dynamics with NAMD. *J. Comput. Chem.* **26**, 1781–1802 (2005).
73. Phillips, J. C. et al. Scalable molecular dynamics on CPU and GPU architectures with NAMD. *J. Chem. Phys.* **153**, 044130 (2020).
74. Huang, J. et al. CHARMM36m: an improved force field for folded and intrinsically disordered proteins. *Nat. Methods* **14**, 71–73 (2017).
75. Klauda, J. B. et al. Update of the CHARMM all-atom additive force field for lipids: validation on six lipid types. *J. Phys. Chem. B* **114**, 7830–7843 (2010).
76. Ryckaert, J.-P., Ciccotti, G. & Berendsen, H. J. C. Numerical integration of the cartesian equations of motion of a system with constraints: molecular dynamics of n-alkanes. *J. Comput. Phys.* **23**, 327–341 (1977).
77. Martyna, G. J., Tobias, D. J. & Klein, M. L. Constant pressure molecular dynamics algorithms. *J. Chem. Phys.* **101**, 4177–4189 (1994).
78. Feller, S. E., Zhang, Y., Pastor, R. W. & Brooks, B. R. Constant pressure molecular dynamics simulation: The Langevin piston method. *J. Chem. Phys.* **103**, 4613–4621 (1995).
79. Darden, T., York, D. & Pedersen, L. Particle mesh Ewald: an N-log(N) method for Ewald sums in large systems. *J. Chem. Phys.* **98**, 10089–10092 (1993).
80. Kästner, J. Umbrella sampling. *WIREs Comput. Mol. Sci.* **1**, 932–942 (2011).
81. Grossfield, A. WHAM: the weighted histogram analysis method, version XXXX, http://membrane.urmc.rochester.edu/wordpress/?page_id=126.

Acknowledgements

The authors thank members of the Accardi lab for helpful discussions. The work was supported by National Institutes of Health (NIH) grants R01-GM128420 (to A.A.), R01-GM106569 and NINDS R24 NS104617 (to C.A.A.), R01-GM123455 and P41-GM104601 (to E.T.). Simulations in this study have been performed using allocations at National Science Foundation Supercomputing Centers (XSEDE grant number MCA06N060), and the Blue Waters Petascale Computing Facility of National Center for Supercomputing Applications (NCSA) at University of Illinois at Urbana-Champaign, which is supported by the National Science Foundation (awards OCI-0725070 and ACI-1238993) and the State of Illinois.

Author contributions

L.L., K.L., S.D., C.A.A., E.T. and A.A. designed experiments; L.L., K.L., S.D., E.F. and J.D.G. performed experiments; L.L., K.L., S.D., E.T. and A.A. analyzed the data; A.A. prepared an initial draft and all authors edited the manuscript.

Competing interests

The authors declare no competing interests.

Additional information

Supplementary information The online version contains supplementary material available at <https://doi.org/10.1038/s41467-022-35279-1>.

Correspondence and requests for materials should be addressed to Alessio Accardi.

Peer review information *Nature Communications* thanks Ben Corry and the other, anonymous, reviewer(s) for their contribution to the peer review of this work. Peer reviewer reports are available.

Reprints and permissions information is available at <http://www.nature.com/reprints>

Publisher's note Springer Nature remains neutral with regard to jurisdictional claims in published maps and institutional affiliations.

Open Access This article is licensed under a Creative Commons Attribution 4.0 International License, which permits use, sharing, adaptation, distribution and reproduction in any medium or format, as long as you give appropriate credit to the original author(s) and the source, provide a link to the Creative Commons license, and indicate if changes were made. The images or other third party material in this article are included in the article's Creative Commons license, unless indicated otherwise in a credit line to the material. If material is not included in the article's Creative Commons license and your intended use is not permitted by statutory regulation or exceeds the permitted use, you will need to obtain permission directly from the copyright holder. To view a copy of this license, visit <http://creativecommons.org/licenses/by/4.0/>.

© The Author(s) 2022